Representation of the Poincaré sections via Dormand–Prince8 (5, 3)* algorithm

A. A. Amara
Department of Physics, College of Sciences, University of Basrah, Basrah, Iraq.

ISSN –1817 –2695
(Received 5/3/2007, Accepted 4/6/2007)

Abstract

This paper deals with the Dormand-Prince 8(5,3) algorithm to analyze two classical nonlinear systems, namely the parametrically damped pendulum and driven damped oscillator , and represents the *Poincaré* sections in two different ways. The *basin of attraction* illustrates the changing of the status for the system according to the choosing of the initial conditions. Many of algorithms like Euler, Runge-Kutta 2&4, Runge-Kutta Fehlberg, Extrapolation, Cash-Karp, Adams-Bashforth-Moulton4, Gear & Implicit Gear, Hamming, Milne and Heun show unstable solutions for our systems. The Dormand-Prince8(5,3) algorithm shows a stable solution for big values of integration step size of the time, in comparison with other algorithms.

Key words: *Poincaré* sections, *Basin of attraction*, Pendulum, Oscillator, Dormand–Prince.

Introduction

In a dynamical system, the is world observed as a function of time. The observations expressed as numbers and record how they change with time; given sufficiently detailed information and understanding of the underlying natural laws, a state of a physical system, at a given instant in time, can be represented by a single point in an abstract space called state space or phase space ***(M)***. As the system changes, so does the representative point in phase space. It is referred to the evolution of such points as dynamics, and the function $\boldsymbol{f}^{\boldsymbol{t}}$, which specifies where the representative point is at time ***t*** as the evolution rule. The most successful class of rules for describing natural phenomena is differential equations. In state space of two (or more) dimensions for dynamical systems, a new type of behavior can arise: motion on a limit cycle. The obvious question is the motion on the limit cycle stable. If the system slightly pushed away from the limit cycle, does it return (at least asymptotically) or is it repelled from the limit cycle? In actual systems both possibilities occur. The stability of limit cycle can be clarified by calculate characteristic values involving derivatives of the functions describing the state space evolution. In principle, one could do this, but *Poincaré* showed that an algebraically and conceptually much simpler method suffices. This method uses what is called a *Poincaré* section of the limit cycle [1].

Usually we want to know the fate of a system for long times, like, will the planets eventually collide or will the system persist for all times? The time of a dynamical system can be either continuous or discrete. Discrete time dynamical systems arise naturally from flows [2]; one can observe the flow at fixed time intervals (by storing it), or one can record the coordinates of the flow when a special event happens (the *Poincaré* section method). This triggering event can be as simple as vanishing of one of the coordinates, or as complicated as the flow cutting through a curved hypersurface. The *Poincaré* section method allows us to characterize the possible type of limit cycles and to recognize the kinds of changes that take place in those limit cycles [3].

*** This integration code is based on the embedded Runge-Kutta method of order 8 with automatic step size control, developed by Prince and Dormand in 1981, as described in [4].**

To understand the dynamics of parametrically damped pendulum and driven damped oscillator, they are essential to simulate it numerically. This can be done by using different algorithms , but the Dormand-Prince8(5,3) algorithm [4] is superior than Euler , Runge-Kutta 2&4 , Runge-Kutta Fehlberg , Extrapolation , Cash-Karp , Adams-Bashforth-Moulton 4 ,Gear & Implicit Gear , Hamming ,Milne and Heun ,wherefrom conversion and stability of the solution ,according to special initial conditions .
In general, *Poincaré* sections method needs to solve the differential equation numerically on the wide range of the time [5] - [11], and this caused serious problems in computational procedure [12].
We try to find a suitable treatment that avoids the conversion and stability problems.

Theory and Numerical Procedure

1 - The parametrically damped pendulum :

Simth and Blackburn have studied this system [13], the equation of motion is,

$$\ddot{\theta} + Q^{-1}[1 + \varepsilon \sin(\Omega(t - \delta))]\dot{\theta} + \sin(\theta) = 0 \qquad (1)$$

Where **(Q , ε , Ω , δ)** are constants .
Poincaré sections in this system represent by drawing **θ** vs **dθ/dt** at certain value of the time, as
$t = 2\pi n / \Omega$, where **n = 1, 2 ,..... N_{max}**, for high-resolution *Poincaré* sections **$N_{max} \sim 10^6$,** and the values of **θ** restricted in the closed interval **[- π , π],** by subtracting or adding **2πm,** where **m** is an integer number.

2 - The driven damped oscillator :

Buskirk and Jeffries have studied this system [14]; the equation of motion is,

$$\ddot{y} + a\dot{y} + e^{y} - 1 = A\sin(t) \qquad (2)$$

Where (**a , A)** are constants .
Poincaré sections in this system represent by drawing **y** vs **dy/dt** at certain value of the time, as
$t = 2\pi n$, where **n = 1, 2,..... N_{max}**, for high-resolution *Poincaré* sections **$N_{max} \sim 10^6$.**

Simth and Blackburn method depend on Fourth order Runge-Kutta algorithm to represent *Poincaré* sections, but Buskirk and Jeffries did not say which algorithm that they depend on.
Our procedure for integrate equations (1) and (2) numerically consist of testing the following algorithms:

1 – Euler	2 – Heun
3 – Runge Kutta 2	4 – Runge Kutta 4
5 – Runge Kutta Fehlberg	6 – Extrapolation
7 – Cash Karp	8 – Adams Bashforth Moulton 4
9 – Gear	10 – Implicit Gear
11 – Hamming	12 – Milne

13 – Dormand Prince 8(5, 3)
In addition, the comparison of the 12th algorithms with Dormand – Prince 8(5, 3) wherefrom conversions and stability of the solution, according to special initial conditions.
We focused on Runge – Kutta 4 and Runge – Kutta Fehlberg algorithm because of the popularity of using them in the numerical simulation [15] – [20].
The mathematical properties of all 13th algorithms summarized in table (1) [4]:

Table(1) mathematical properties of algorithms.

Algorithm	Type	Step size	Interpolation
Dormand-Prince8(5,3)	embedded Runge-Kutta	variable	7^{th} order polynomial
Extrapolation	extrapolation	variable	Hermite (3^{rd} order)
Cash-Karp	embedded Runge-Kutta	variable	Hermite (3^{rd} order)
Runge Kutta Fehlberg	embedded Runge-Kutta	variable	Hermite (3^{rd} order)
Implicit Gear	Implicit	variable	Hermite (3^{rd} order)
Gear	predictor – corrector	fixed	Hermite (3^{rd} order)
Hamming	predictor – corrector	fixed	Hermite (3^{rd} order)
Runge – Kutta 4	Runge-Kutta	fixed	Hermite (3^{rd} order)
Adams Bashforth Moulton 4	predictor – corrector	fixed	Hermite (3^{rd} order)
Milne	predictor – corrector	fixed	Hermite (3^{rd} order)
Runge Kutta 2	elementary	fixed	Linear (1^{st} order)
Heun	elementary	fixed	Linear (1^{st} order)
Euler	elementary	fixed	Linear (1^{st} order)

Results and Discussion

Numerical solutions of equations (1) and (2) were obtained with several algorithms , and the tolerance appropriate with $\mathbf{10^{-15}}$ for parametrically damped pendulum and $\mathbf{10^{-25}}$ for driven damped oscillator , for Fig (1) – Fig (10) and the initial conditions are :

1) $\boldsymbol{\theta(0) = 0}$ and $\boldsymbol{(d\theta/dt)_{t=0} = -5}$.

2) $\boldsymbol{y(0) = -15}$ and $\boldsymbol{(dy/dt)_{t=0} = -24}$.

With the parameters $\mathbf{Q = 18.33, \varepsilon = 19.8 , \delta = 27^{0} , a = 0.05}$ **and** $\mathbf{A = 2}$. These parameters were chosen in accordance with those in [13] and [14] respectively, but $\boldsymbol{\Omega}$ here equal to **1.81**.

For Fig (11) and Fig (12) the tolerance appropriate with $\mathbf{10^{-25}}$, these figures show the values of ($\mathbf{t_c}$ critical time) obey to the following relation :

$\mathbf{t_c}$(Dormond-Prince8(5,3)) > $\mathbf{t_c}$(Runge-Kutta Fehlberg) > $\mathbf{t_c}$(Runge-Kutta 4) .....(3)

Superiority of Dormand-Prince8(5,3) on the most popular algorithms, Runge-Kutta Fehlberg and Runge-Kutta 4 is shown in Figs(11) and (12), and these are valid for Fig (1) to Fig (10) , so that , $\mathbf{t_c}$(Dormand-Prince8(5,3))> $\mathbf{t_c}$(all 10^{th} algorithm) ,in order to reach for high resolution *Poincaré* sections, this seek a big value of time , so that ,

t (high resolution) >> $\mathbf{t_c}$ ……...(4)

For big value of **t**, stability and conversion of the solution needs to:

1- Tolerance of the solution << $\mathbf{10^{-25}}$.

2- Upper bound of the inequality ($\mathbf{h_{min} < h < h_{max}}$) for integration step size is ($\mathbf{h_{max} << 10^{-10}}$) .

3- Under these considerations, expected run time reaching to very big value.

Our cogitation to avoid the complicating of computational procedure for ($\mathbf{t >> t_c}$) , is :

1- Choosing value of the time like ($\boldsymbol{\tau < t_c}$) .

2- Solve equations (1) and (2) on the interval $\boldsymbol{[\,0, \tau\,]}$, and change the initial conditions like : $\boldsymbol{\alpha < (d\theta/dt)_{t=0} < \beta}$ **,** $\boldsymbol{\theta(0)}$ is a constant , $\boldsymbol{a_1 < (dy/dt)_{t=0} < a_2}$ **,** $\boldsymbol{y(0)}$ is a constant .

3- Draw $\boldsymbol{\theta(t = \tau)}$ vs $\boldsymbol{(d\theta/dt)_{t=\tau}}$, $\boldsymbol{y(t = \tau)}$ vs $\boldsymbol{(dy/dt)_{t=\tau}}$, for each initial conditions .

4 - $\boldsymbol{\alpha}$, $\boldsymbol{\beta}$, $\boldsymbol{a_1}$ and $\boldsymbol{a_2}$ should be choosing carefully, in order to save the run time .

Fig (13 – a) Poincaré sections show self-similarity and fractal structure, **y** vs **dy/dt** , storing at $\mathbf{t = 2\pi N, N = 1,2,….,2 \times 10^{6}}$, from numerical solutions of equation (2) , boxed region of the strange attractor , magnified in Fig(14 – a) .

Fig(13 – b) *Poincaré* sections in case of changing the initial conditions, from numerical solutions of equation (2) , boxed region of the strange attractor , magnified in Fig(14 – b) .

Fig(15 – a) *Poincaré* sections , θ vs $d\theta/dt$, stored at $t = 2\pi N/\Omega$, $N = 1,2,\ldots,10^6$, from numerical solutions of equation (1) , boxed region of the strange attractor , magnified in Fig(16 – a) .

Fig(15 – b) *Poincaré* sections in case of changing the initial conditions, from numerical solutions of equation (1) , boxed region of the strange attractor , magnified in Fig(16 – b) .

Figures (13 – b) , (14 – b) , (15 – b) and (16 – b) shows the similarity with Figures (13 – a) , (14 – a) , (15 – a) and (16 – a) .

Fig(17) *Poincaré* sections , **y** vs **dy/dt** , stored at $t = 2\pi N$, $N = 1,2,\ldots,10^5$, from numerical solutions of equation (2) , boxed region of the strange attractor magnified , $y(0) = -15$, $(dy/dt)_{t=0} = -24$.

Fig(18) *Poincaré* sections , θ vs $d\theta/dt$, stored at $t = 2\pi N/\Omega$, $N = 1,2,\ldots,10^5$, with several values of phase shift δ , from numerical solutions of equation (1) .

The choice of initial conditions then determines which of the attractors selected by the system. This is illustrated by the *basin of attraction* presented in Fig(19) ; it is essentially a map of the outcome of trying all combinations of **1000** different $\theta(0)$ with **1000** values of $(d\theta/dt)_{t=0}$ over the ranges indicated . For each of the 10^6 initial conditions, equation (1) solved over a total time span covering 55 modulation cycles. The first 50 cycles were discarded to eliminate transient effects, and the behavior in the remaining five cycles was examined. The figure vividly indicates the complexity of even this nonchaotic motion. Although there is a uniform region surrounding the origin in which a stationary state is ultimately reached, the structure elsewhere appears to be fractal. Fractally intermixed basins have already been observed for forced pendulum, and for the radiofrequency (rf)-driven Josephson junction [13]. Fig(19) Basin of attraction for $Q = 18.33$, $\varepsilon = 6$, $\delta = 0$, and $\Omega = 1.7$ **,** the computational grid is **1000x1000** points. Black areas denoted stationary states .Blank areas are periodic, or multiperiodic.

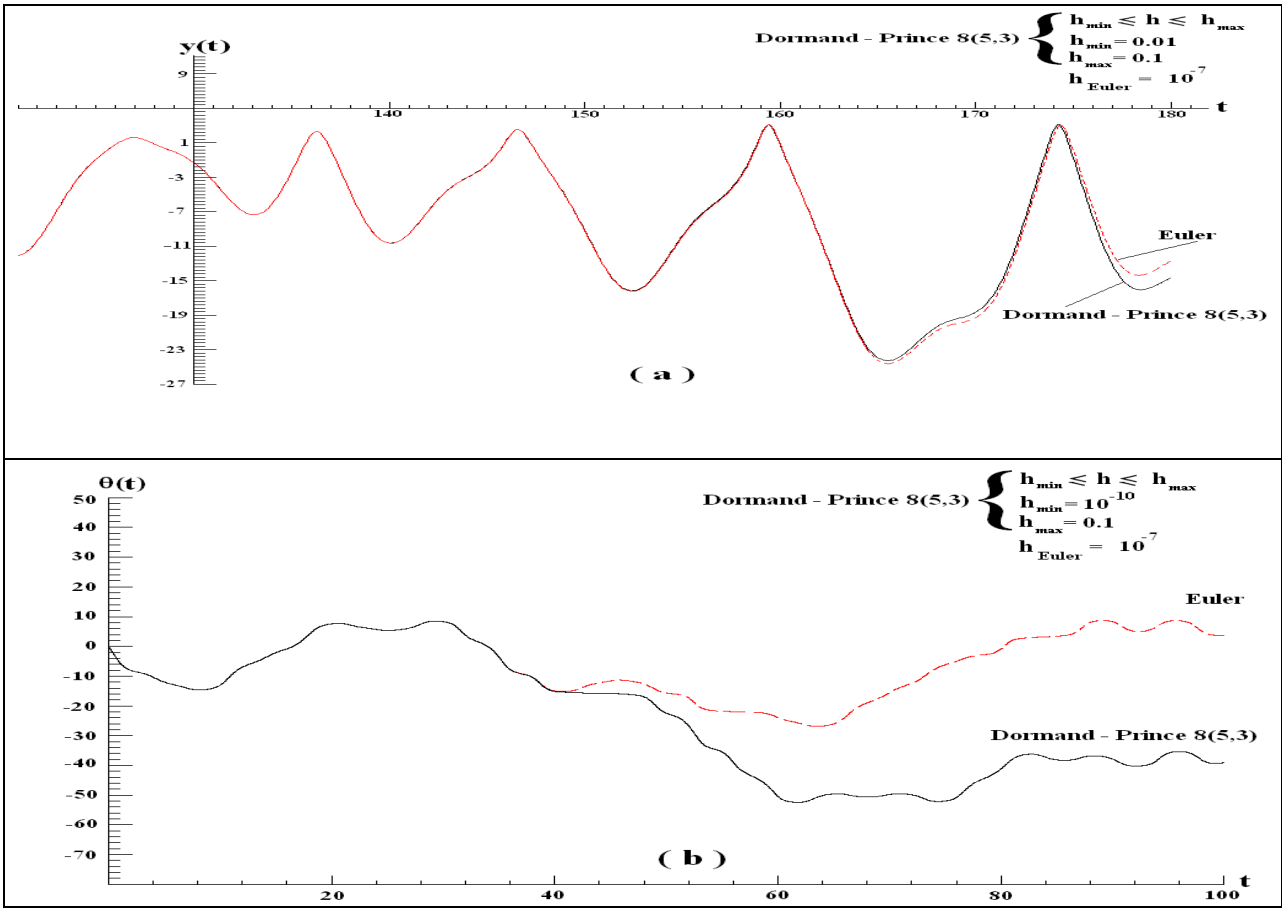

Figure (1 – a, b) solutions of equations (2) and (1) via Euler and Dormand-Prince8 (5, 3).

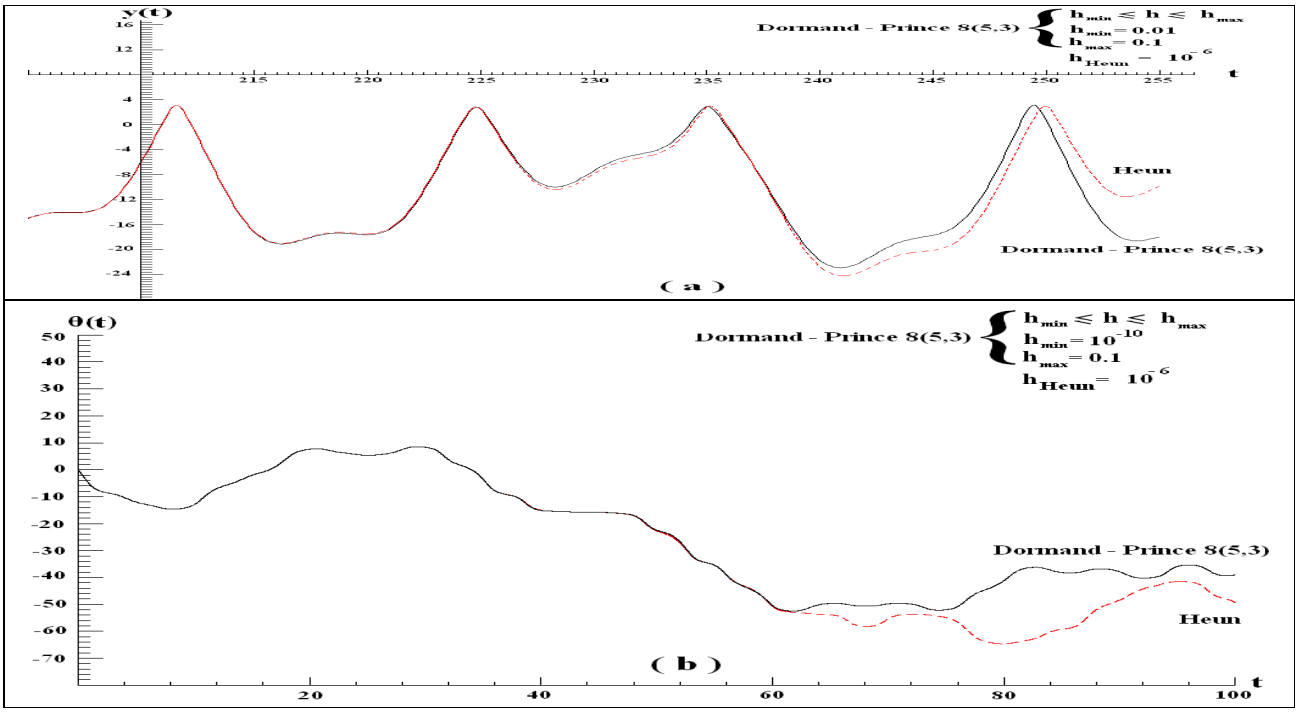

Figure (2 – a, b) solutions of equations (2) and (1) via Heun and Dormand-Prince8 (5, 3).

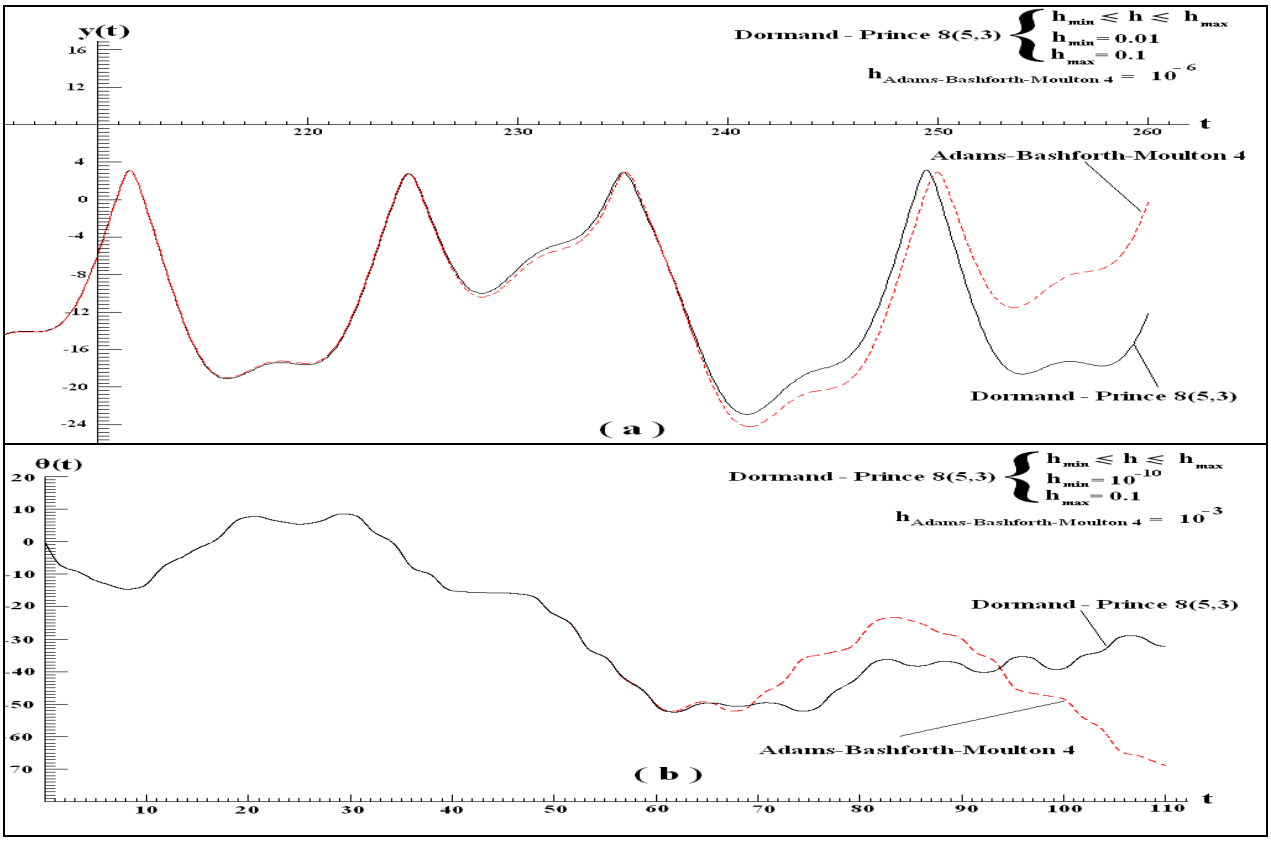

Figure (3 – a, b) solutions of equations (2) and (1) via Adams Bashforth Moulton 4 and Dormand-Prince8 (5, 3).

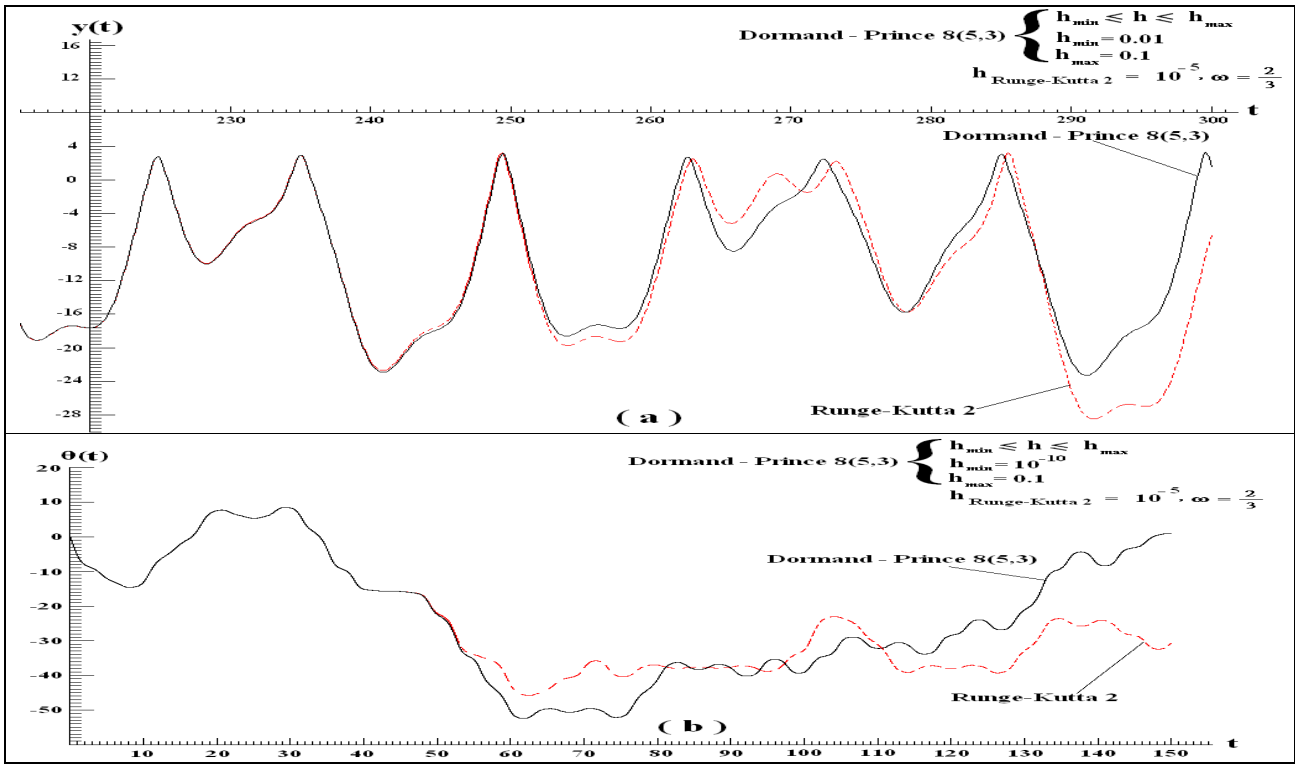

Figure (4 – a, b) solutions of equations (2) and (1) via Runge Kutta 2 and Dormand-Prince8 (5, 3).

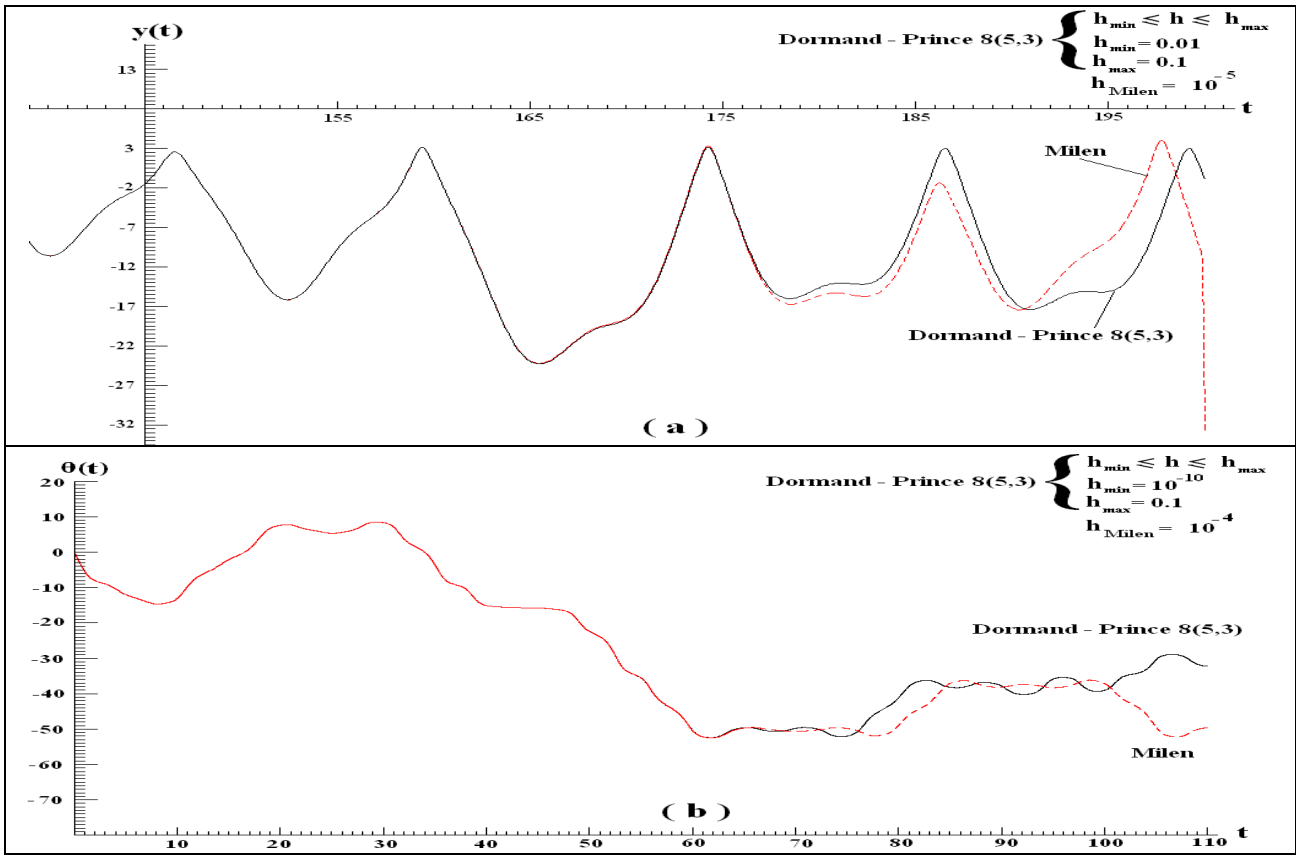

Figure (5 – a, b) solutions of equations (2) and (1) via Milen and Dormand-Prince8 (5, 3).

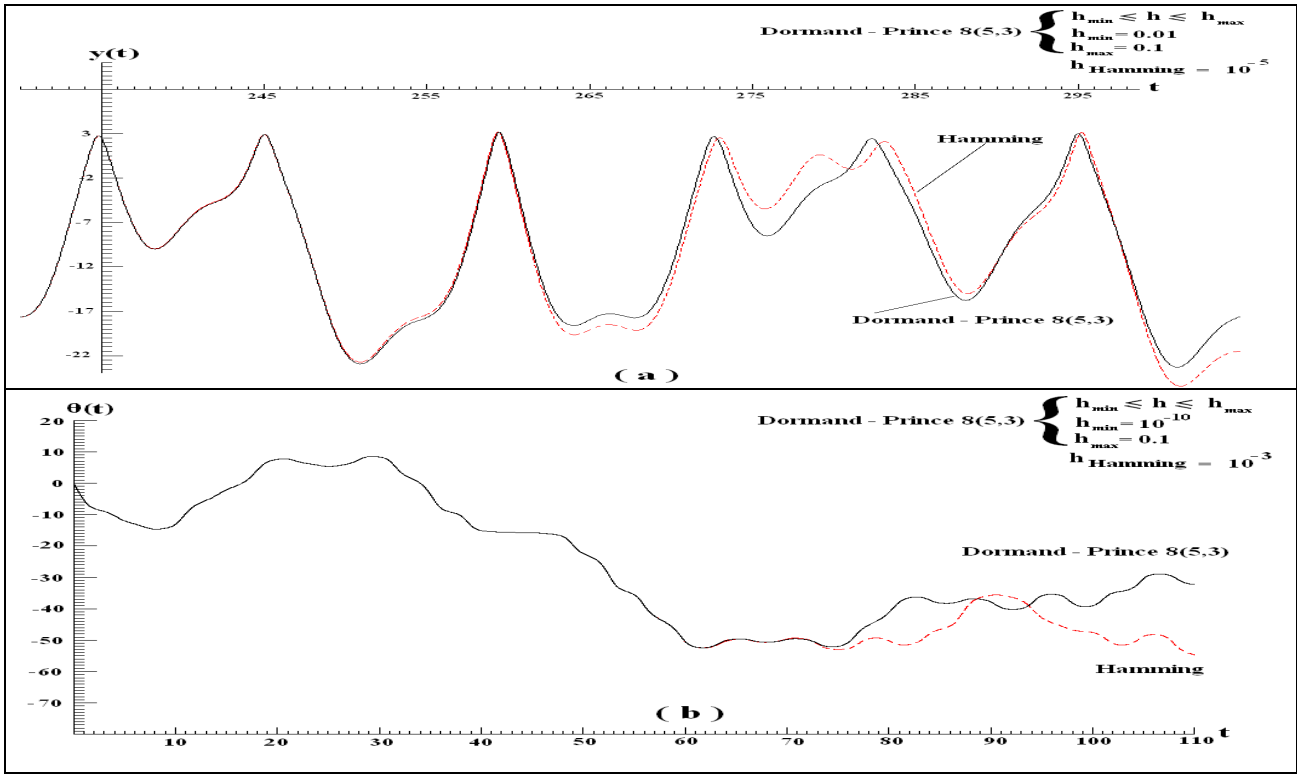

Figure (6 – a, b) solutions of equations (2) and (1) via Hamming and Dormand-Prince8 (5, 3).

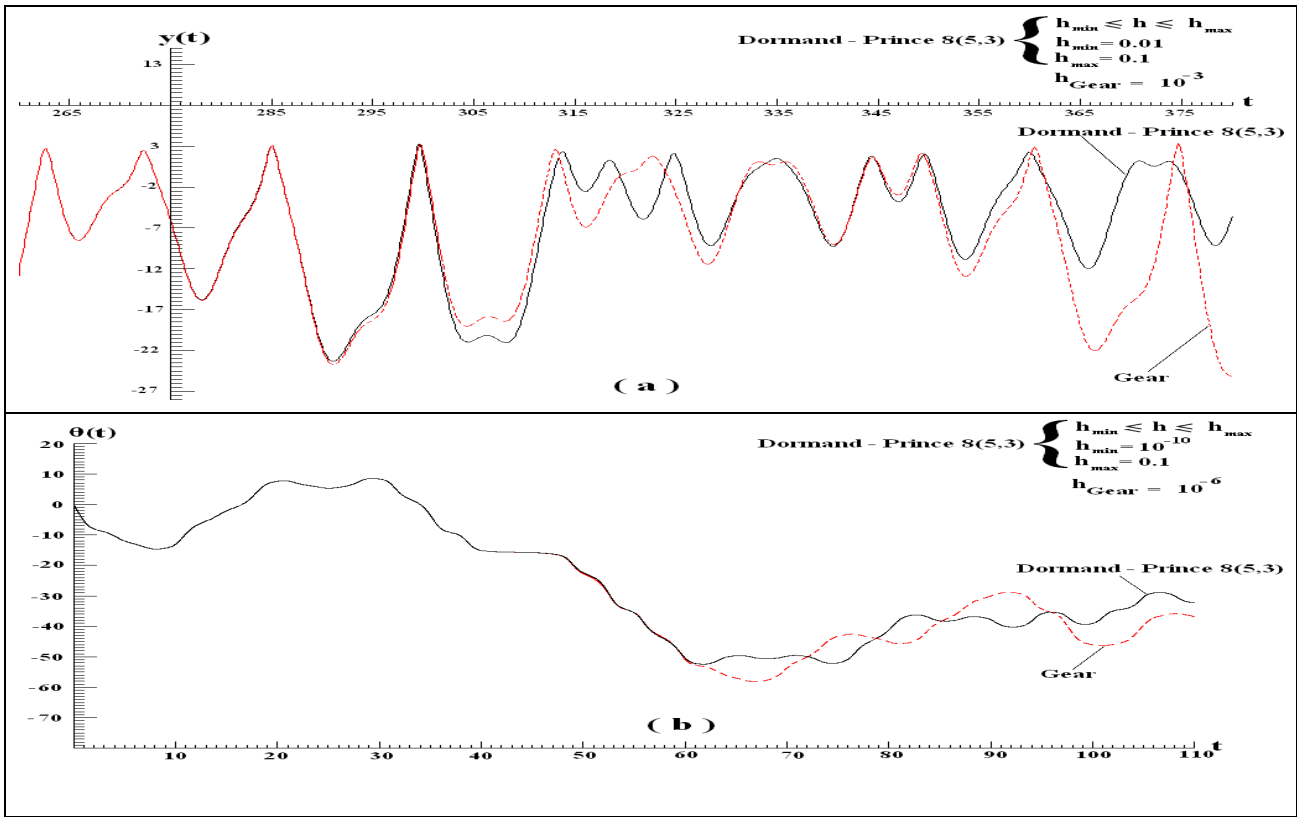

Figure (7 – a, b) solutions of equations (2) and (1) via Gear and Dormand-Prince8 (5, 3).

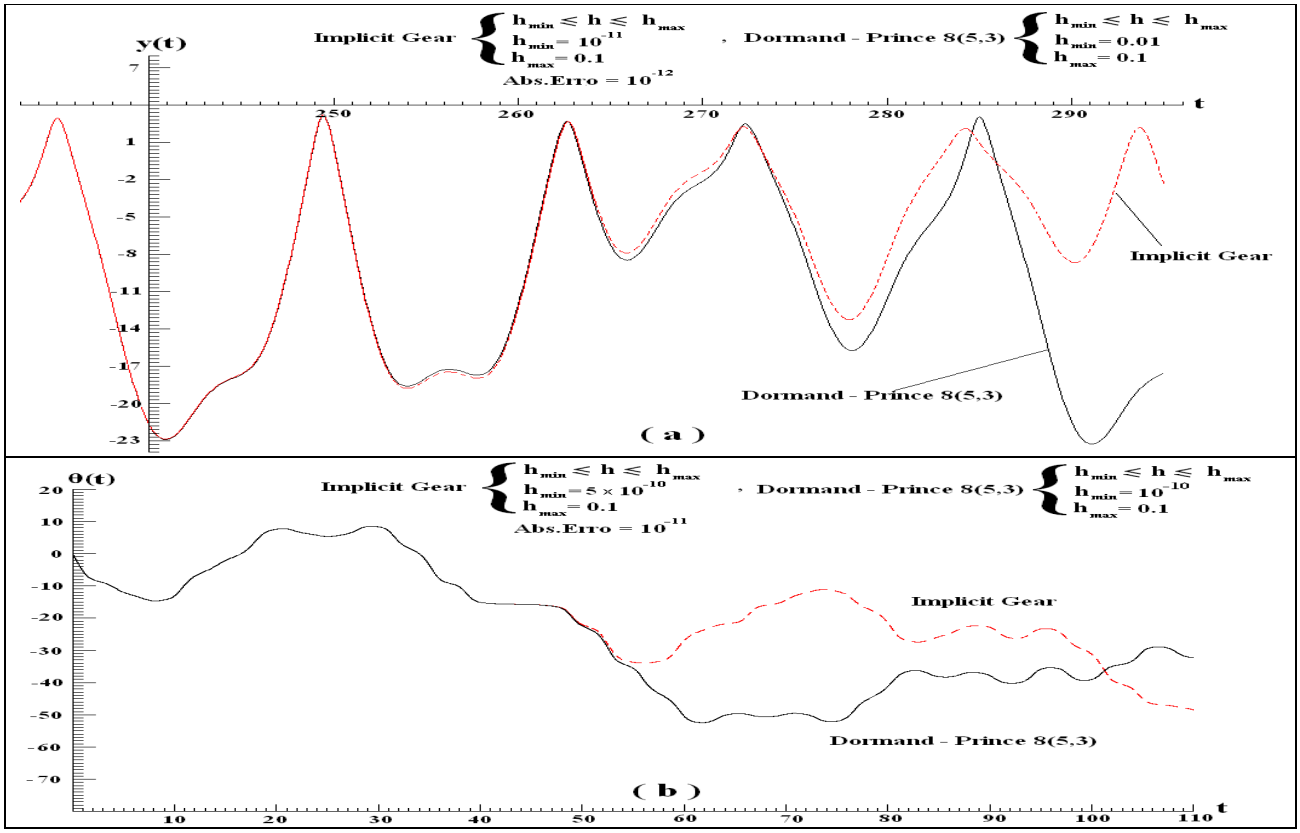

Figure (8 – a, b) solutions of equations (2) and (1) via Implicit Gear and Dormand-Prince8 (5, 3).

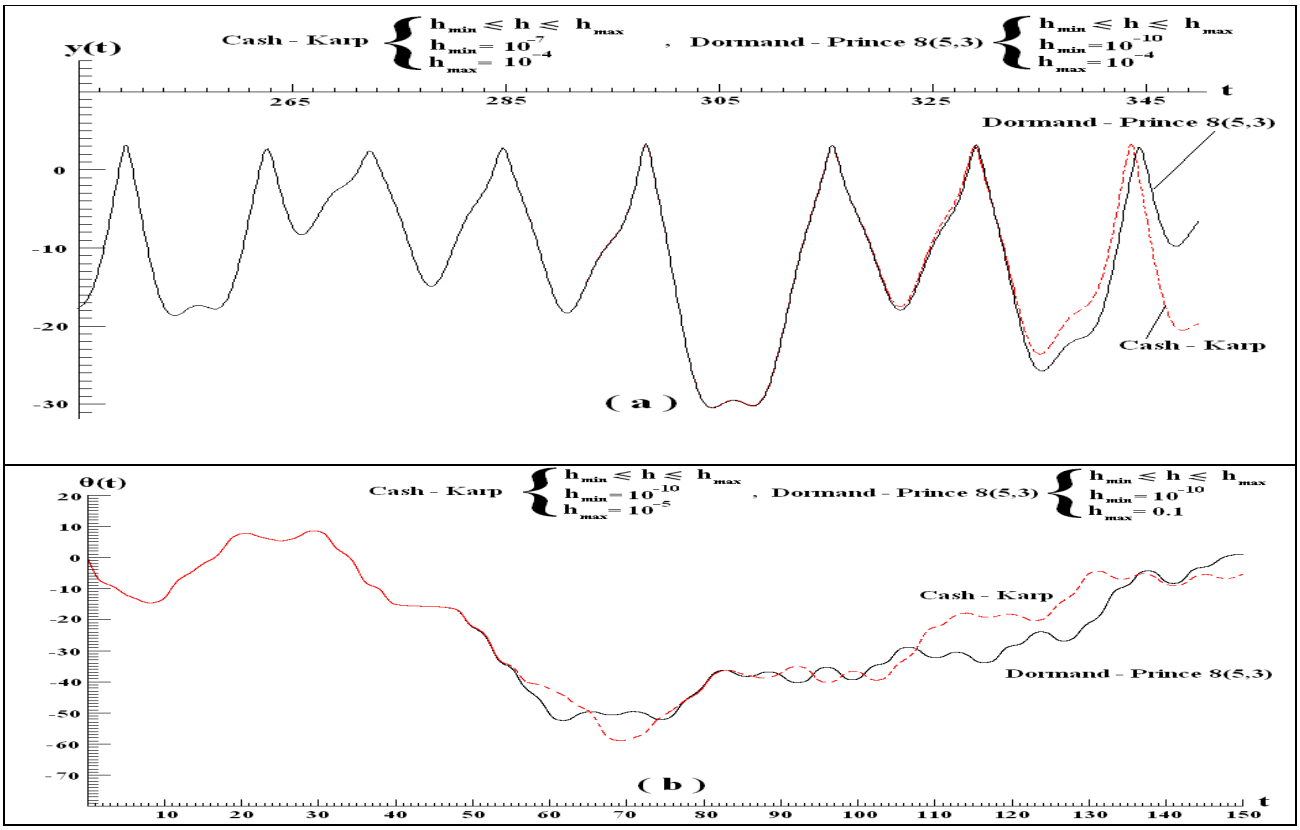

Figure (9 – a, b) solutions of equations (2) and (1) via Cash – Karp and Dormand-Prince8 (5, 3).

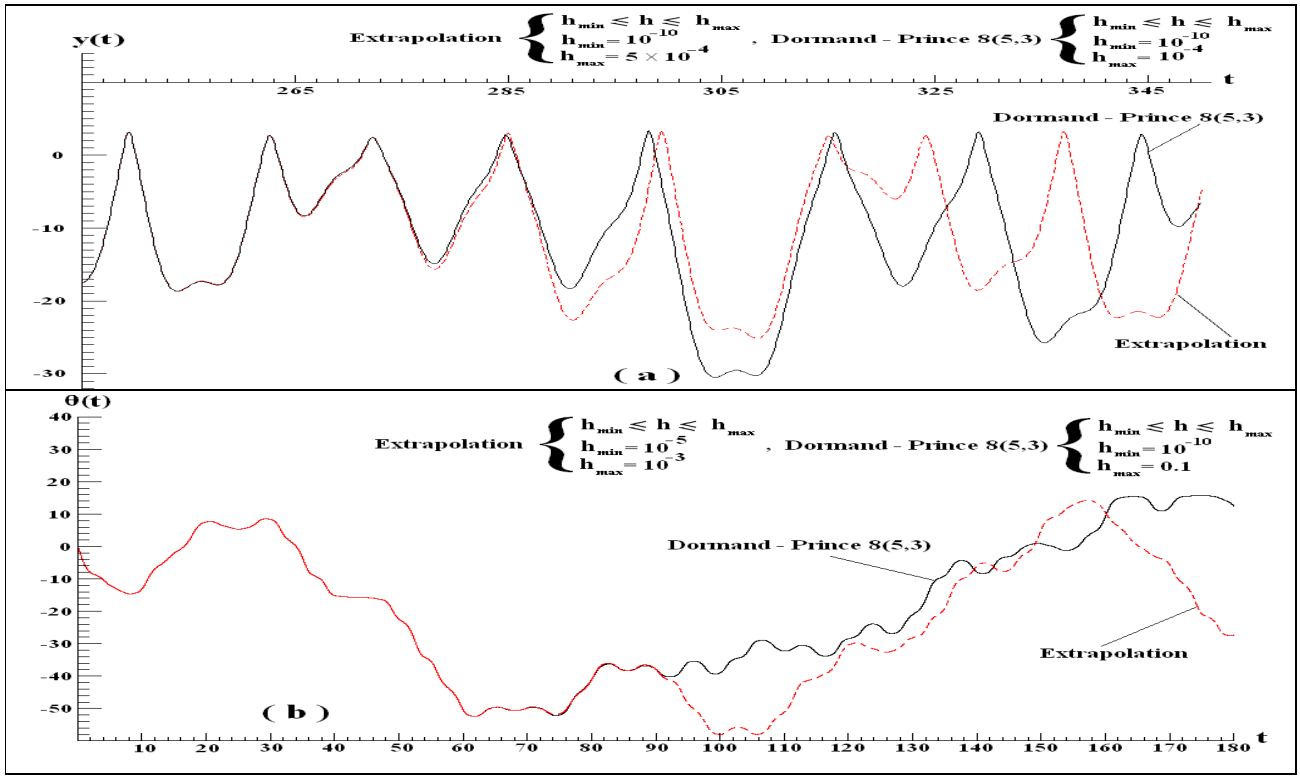

Figure (10 – a, b) solutions of equations (2) and (1) via Extrapolation and Dormand- Prince8 (5, 3).

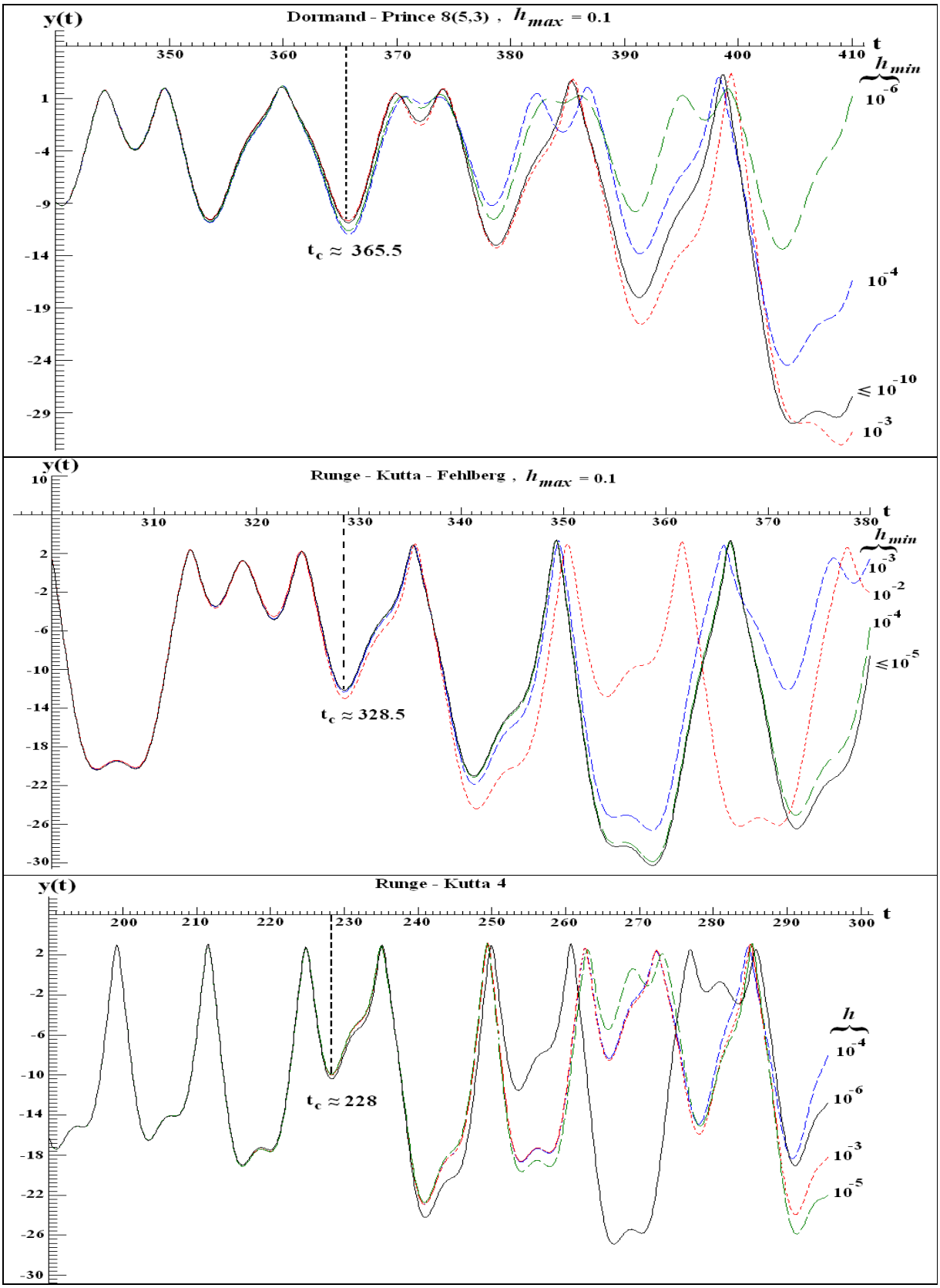

Figure (11) solutions of equation (2) via Runge – Kutta 4, Runge Kutta Fehlberg and Dormand-Prince8 (5, 3).

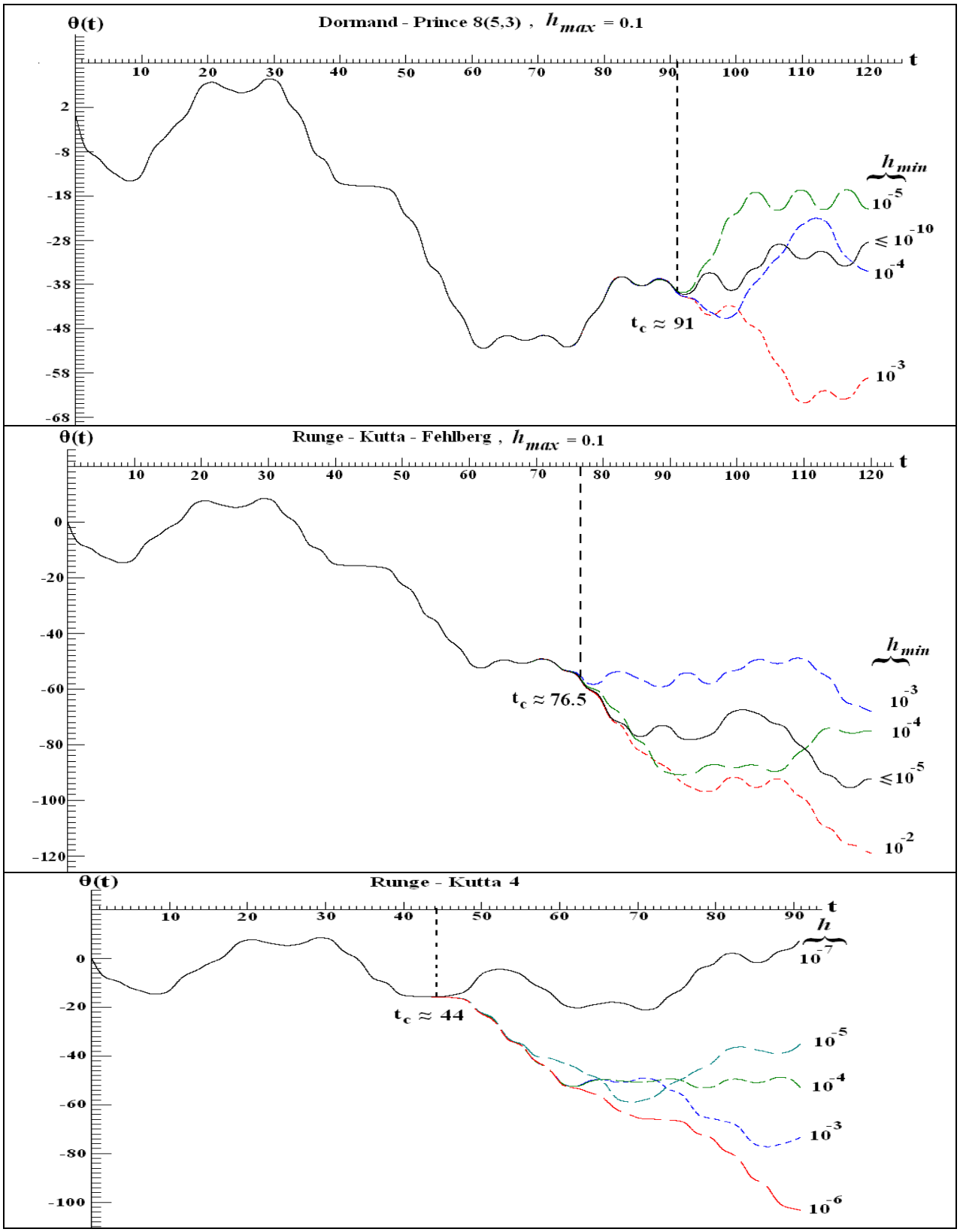

Figure (12) solution of equation (1) via Runge – Kutta 4, Runge Kutta Fehlberg and Dormand-Prince8 (5, 3).

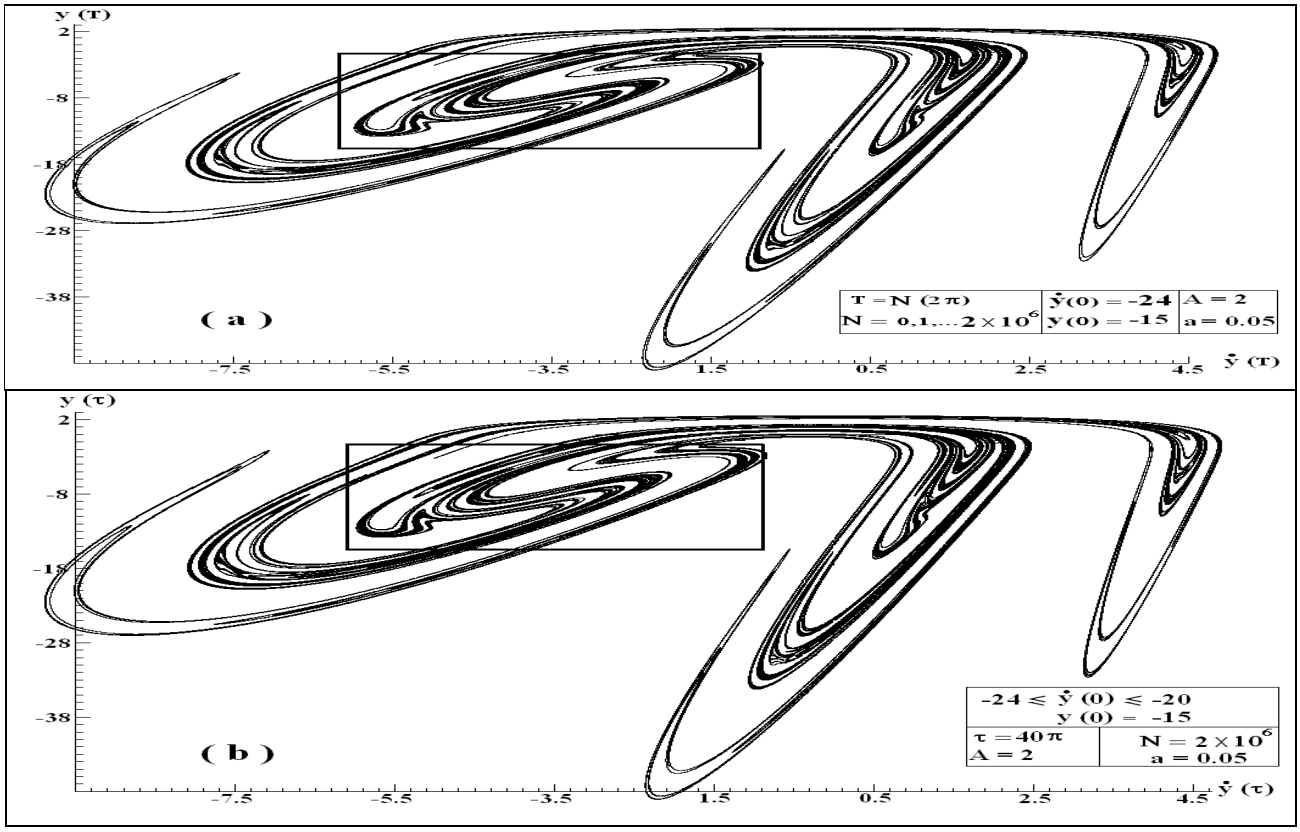

Figure (13 – a) ***Poincaré*** **sections from numerical solutions of equation (2).**
Figure (13 – b) ***Poincaré*** **sections from numerical solutions of equation (2) with $\tau = 40\pi$.**

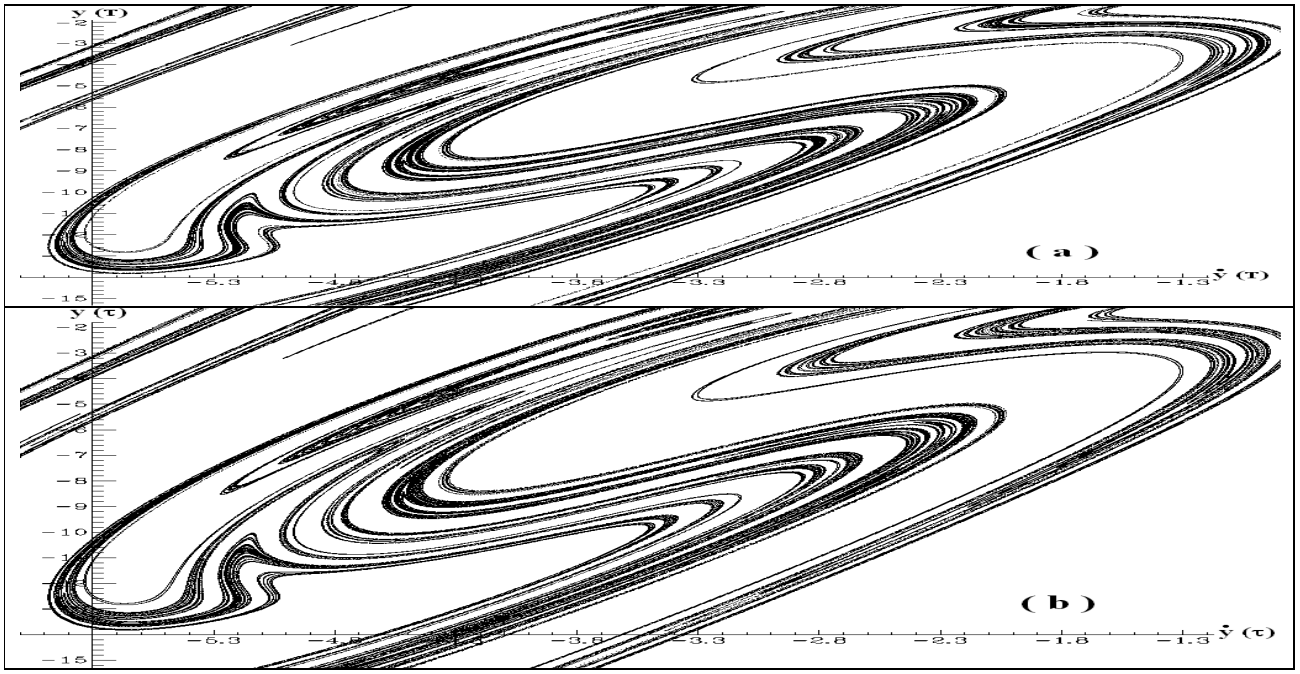

Figure (14 – a, b) magnifying boxed region of Fig (13 – a, b).

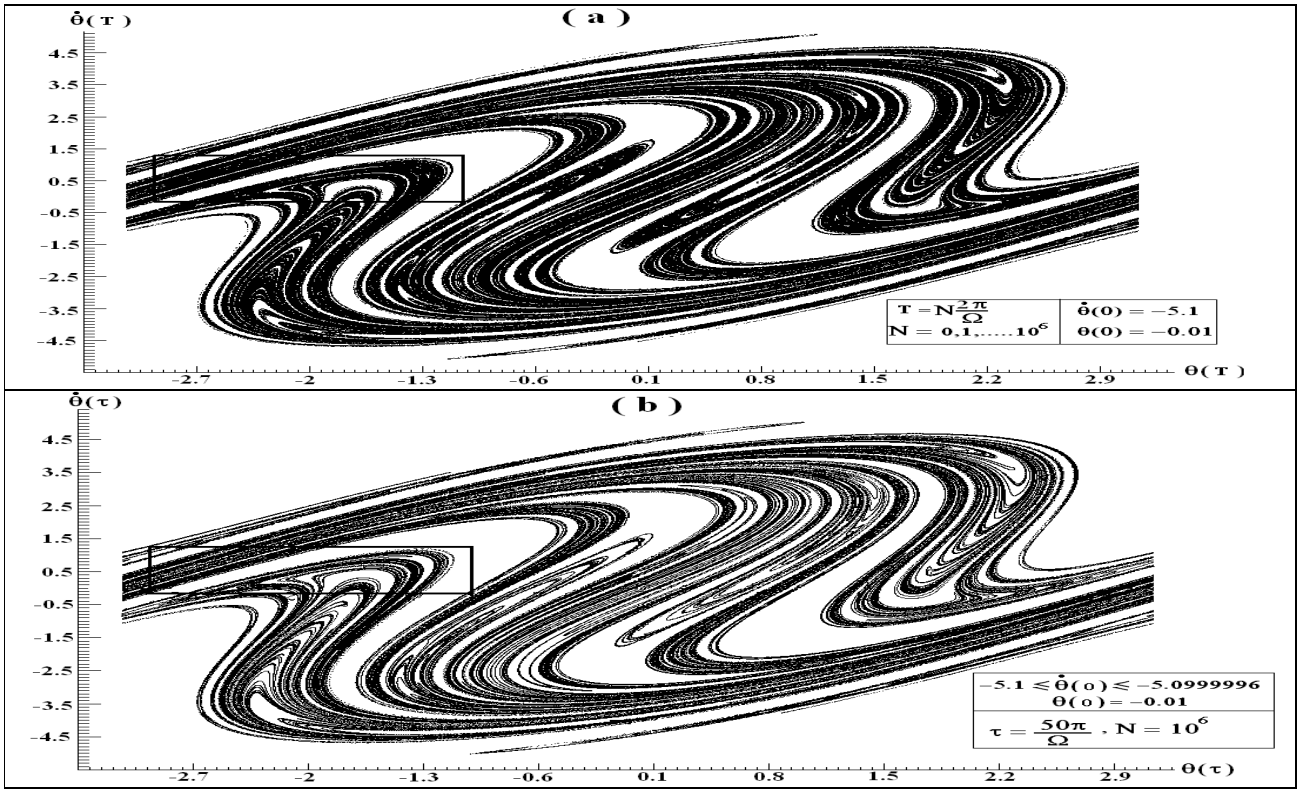

Figure (15 – a) ***Poincaré*** **sections from numerical solutions of equation (1).**
Figure (15 – b) ***Poincaré*** **sections from numerical solutions of equation (1) with $\tau = 50\pi/\Omega$.**

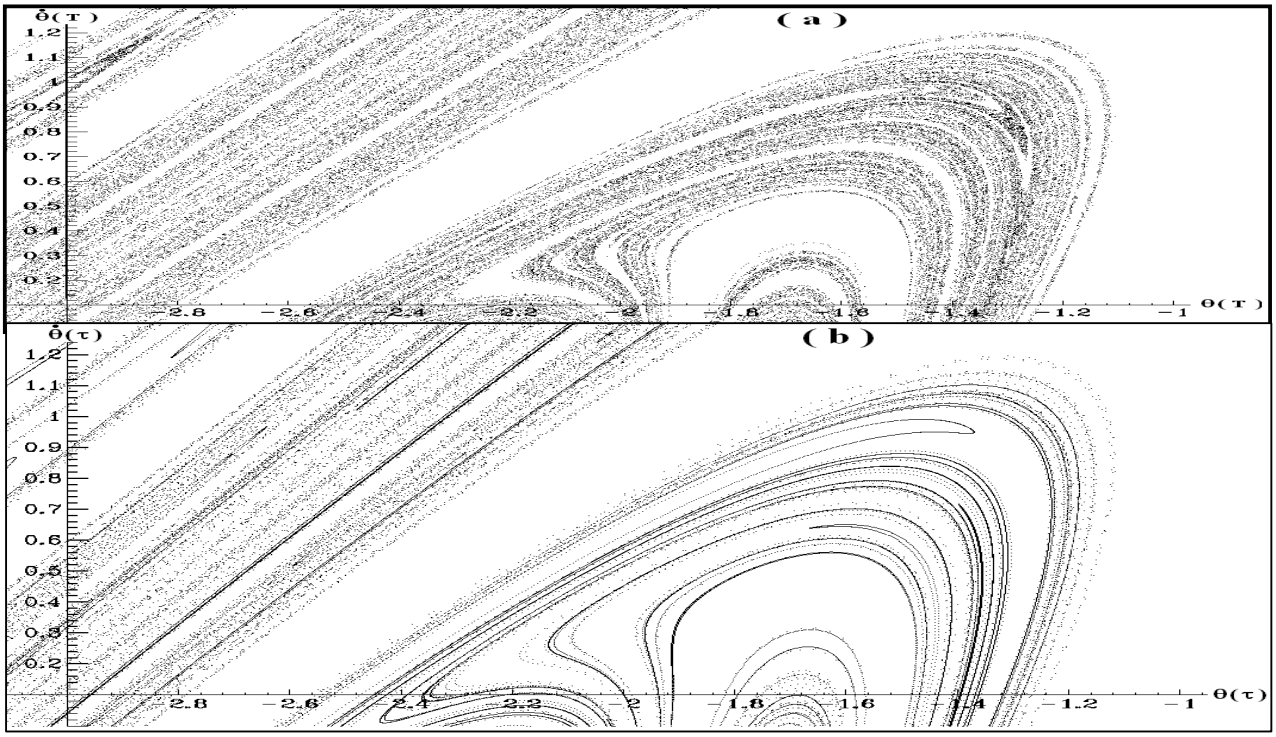

Figure (16 – a, b) magnifying boxed region of Fig (15 – a, b).

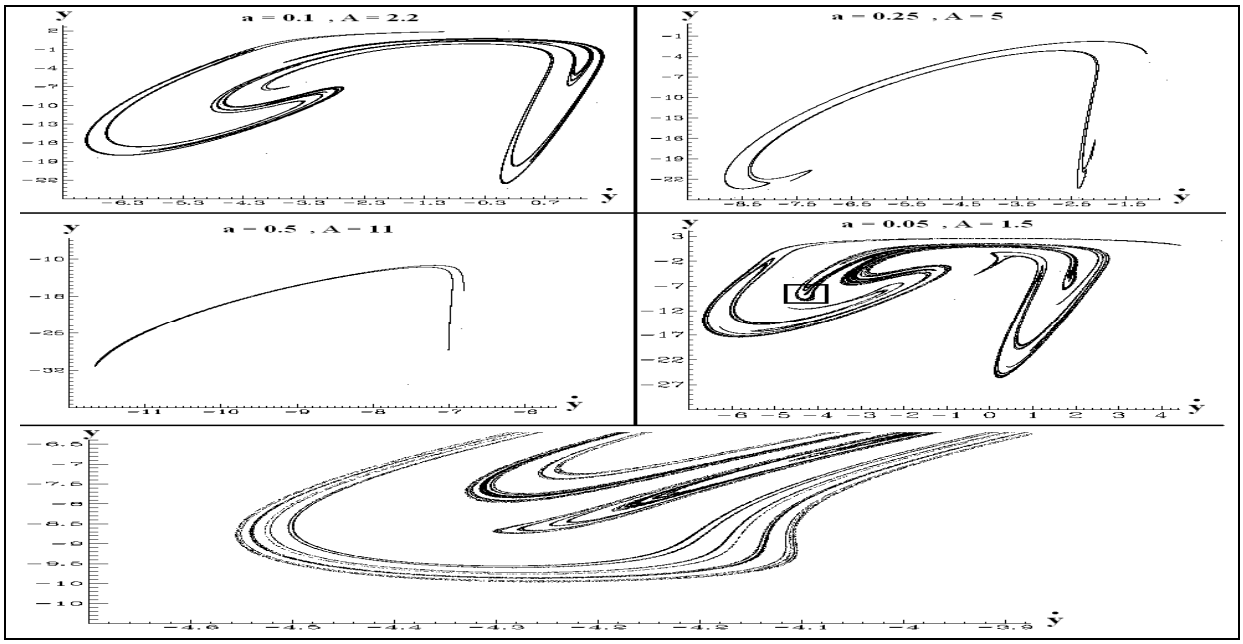

Figure (17) *Poincaré* sections from numerical solutions of equation (2), with several values of (a, A).

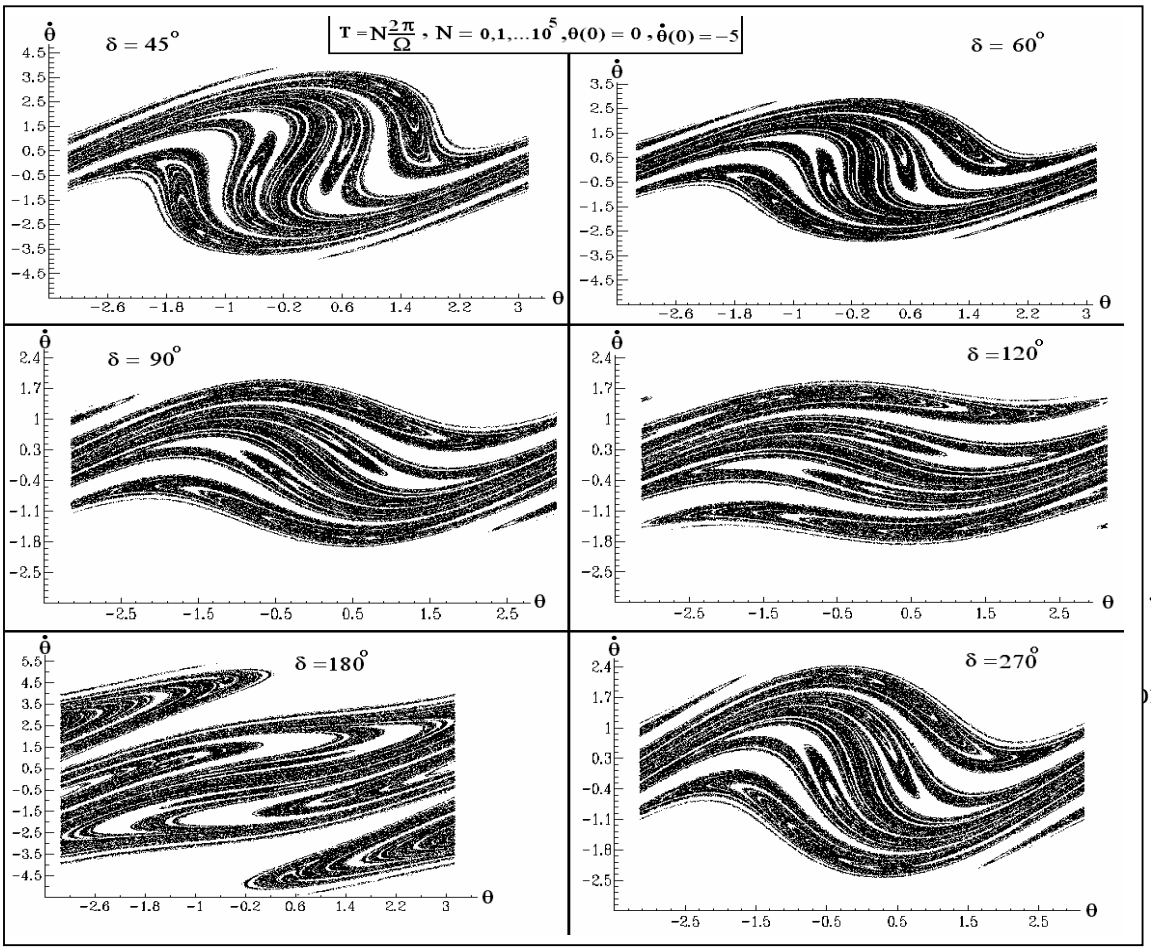

Figure (18) *Poincaré* sections from numerical solutions of equation (1), with several values of δ .

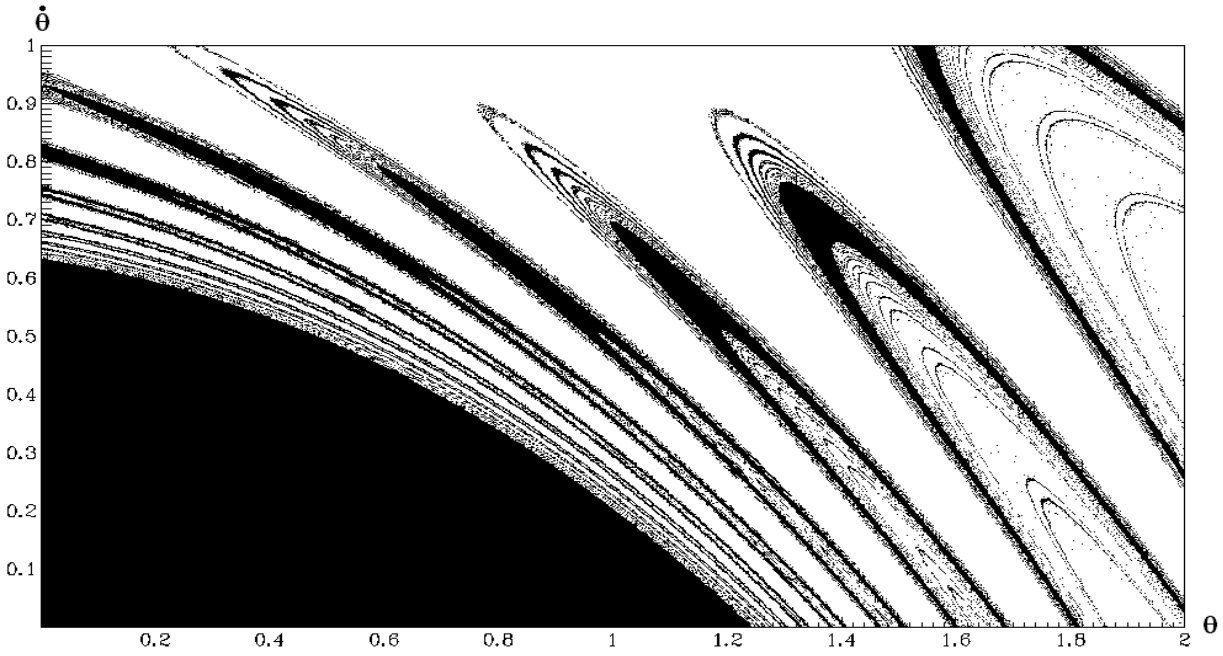

Figure (19) Basin of attraction from numerical solutions of equation (1).

Conclusions

In this study, we can perform the fallowing conclusions:

1 – Dormand-Prince8 (5, 3) is a good choice wherefrom conversion and stability of the solution, when we try to solve a nonlinear ordinary differential equations.

2 – Dormand-Prince8 (5, 3) is faster than other algorithms in case of run time.

3 – Varying the initial conditions is another way to obtain *Poincaré* sections.

4 – The maximum tolerance is less than $\mathbf{10^{-7}}$in order to achieve confidential solutions.

Acknowledgments

I thank C.A. Emshary for his help on some aspects of this work and for fruitful discussions.

References

[1] B. Nicholas, A .Tyler, and P. Reilly, An Experimental Approach to Nonlinear Dynamics and Chaos, Addison – Wesley, (1992).

[2] E. Scheinerman , Invitation to dynamical systems , Prentice – Hall, (2000).

[3] M. V. Bartuccelli , G. Gentile and K. V. Georgiou , Proc. R. Soc. Lond . **A**457,3007.(2001).

[4] E. Hairer, S. P. Norsett and G. Wanner, Solving Ordinary Differential Equations I: Non-stiff Problems, 2nd ed., Springer, Berlin (1993).

[5] L. Shew, A. Coy and F. Lindner , Am. J. Phys. **67**(8),703.(1999).

[6] M. Dubois, Int. J. Comp. Antici. Sys. **14**, 3. (2004).

[7] A. Orlans, M. Sc. thesis, Bristol Univ. (2006).

[8] A. Kim , K. Lee , M. Y. Choi and S. Kim , J. Korean Phys. Soc. **44**(3),518.(2004).

[9] B. Yamrom , I. Kunin , R. Metcalfe and G. Chernykh , Int. J. Engng. Sci. **41**, 449. (2003).

[10] E. I. Butikov , J. Phys. A: Math. Gen. **35,** 6209. (2002).

[11] J.L. Trueba, J.P. Baltanas and M .A. F. Sanjuan, Chaos, Solitons & Fractals. **15**, 911. (2003).
[12] S. Filippi and J. Gräf**,** J. Comp. Appl. Math. **14**,361. (1986).
[13] H. Smith and J. Blackburn, Phys. Rev. A**40**(8), 4708. (1989).
[14] R. Buskirk and C. Jeffries, Phys. Rev. A**31**(5), 3332. (1985).
[15] D. W. Sukow, Ph. D. thesis, Duke Univ. (1997).
[16 W. H. Press, S. A. Teukolsky, W. T. Vetterling, and B. P. Flannery, Numerical Recipes in C++, 2nd ed., Cambridge University Press, New York, (2002).
[17 L. Wang, Ph. D. thesis, Florida Univ. (1996).
[18 P.H. Muir, R.N. Pancer and K.R. Jackson, Parallel Computing **29**,711. (2003).
[19] B. Fix, J. Glimm, Xiaolin. Li, Yuanhua. Li, X. Liu and R. Samulyak, J. Phys. **16**, 471. (2005).
[20] H. E. Nusse and J. A. Yorke , Dynamics : Numerical Explorations , Springer , Berlin (1998).

علي أحمد عمارة

قسم الفيزياء , كلية العلوم , جامعة البصرة , البصرة , العراق

الخلاصة

استخدمنا خوارزمية Dormand-Prince8 (5, 3) لتحليل نظامين كلاسيكيين لا خطيين , وهما البندول المتضائل بارامتريا و المتذبذب المساق المتضائل وتمثيل مقاطع (*Poincaré*) بطريقتين مختلفتين . توضح التغيرات في حالة النظام وفق شروط ابتدائية مختارة من خلال حوض الجذب للنظام. الخوارزميات المستخدمة هنا تعطي حلولاً غير مستقرة للنظامين قيد الدراسة. خوارزمية Dormand-Prince أظهرت حلولاً مستقرة لقيم كبيرة من شرائح التكامل الزمني, بالمقارنة مع بقية الخوارزميات.